SSRG International Journal of Civil Engineering (SSRG-IJCE) – volume 2 Issue 5 May 2015

Parametric Study on the Distribution of Longitudinal Load in Railway Track under Dynamic Wheel Loading using Finite Element Analysis

Zijian Zhang[1], Bassem Andrawes[2], and J. Riley Edwards[3]

[1]*(Department of Civil and Environmental Engineering/ University of Illinois at Urbana-Champaign, USA)*

[2]*(Department of Civil and Environmental Engineering, University of Illinois at Urbana-Champaign, USA, Corresponding author)*

[3]*(Rail Transportation and Engineering Centre (RailTEC), Department of Civil and Environmental Engineering, University of Illinois at Urbana-Champaign, USA)*

ABSTRACT : *The increasing tractive power of locomotives has led to a significant increase in the longitudinal loading demand on railway tracks. The capacity of longitudinal restraint of existing rail fastening system and its dependency on track parameters can affect the future design of the rail fastening system. This paper investigates the effects of wheel acceleration, elastic modulus of clips, rail to rail pad coefficient of friction (COF), and sleeper spacing on the distribution of longitudinal force in the rail fastening system and on the maximum rail to rail pad friction force. A finite element (FE) model with multiple sleepers and their accompanying fastening systems, along with a moving wheel, is developed and validated using field data. The results of our parametric study indicate that a COF of 0.65 is optional when maximizing the longitudinal resistance per rail seat. Additionally, the maximum rail to rail pad friction force increases exponentially with the spacing of sleepers, and a sleeper spacing of 0.61 m can lead to a desired distribution of longitudinal force.*

Keywords *-concrete sleeper, fastening system, finite element analysis, longitudinal load, parametric study*

I. INTRODUCTION

Outside of the realm of thermal forces and expansion, longitudinal forces in a railway track are produced by the tractive effort and dynamic braking of a train [1]. As railway traffic has increased over the past few decades in terms of their tonnages and speed of trains, more powerful locomotives have been built to meet the demands. The latest model of diesel-electric locomotive is capable of producing twice as much tractive force as its predecessors [2]. As a result, the longitudinal forces imparted from the tractive effort are increased significantly. The longitudinal forces transfer from the rail to the sleepers through the fastening system. In other words, the fastening system serves as the connection between the rail and the sleepers, thus anchors the rail against its longitudinal movement due to forces in the longitudinal direction [1]. Therefore, the increase in the wheel-induced longitudinal forces can impose a higher loading demand in the fastening system.

The recommended practices for track component design in the United States is maintained by the American Railway Engineering and Maintenance-of-Way Association (AREMA) and it provides a single-tie and single-rail pullout test as the reference for the design and manufacture of rail fasteners (Figure 1). It states a threshold of 5.08 mm for the longitudinal displacement of the rail as an increasing longitudinal force, up to 10.7 kN, is applied to the rail and held for 15 minutes; and an additional longitudinal displacement of 0.25 mm cannot be exceeded after the force is held for three minutes. A similar test is described in the European standard [3], except for that the longitudinal load is increased until slippage occurs in the rail. As is conducted on a single rail seat, the test specified in [4] only accounts for a longitudinal force that is not greater than 10.7 kN per rail seat. The value of 10.7 kN, according to AREMA [4], is sufficient considering normal service conditions, but there are locations where excessive longitudinal forces are expected. In addition, the test only applies to fasteners on sleepers with 0.61-m spacing. Therefore, the longitudinal load imparted in the rail seat under various service conditions needs to be investigated.

In field experimentation conducted by Srinivas et al. [1], longitudinal track forces on a bridge was investigated. The field experimentation focused on the scenarios that include the accelerating and braking of a train as well as the train running at uniform speeds. Based on the results of the experimentation, among the three testing scenarios, the highest longitudinal force is imparted in the rail under the passage of an accelerating train. Furthermore, a much more

significant longitudinal force is induced by the locomotive wheel compared to the trailing railcar wheels [1]. As illustrated in Figure 2, a locomotive wheel is driven by the rotation of the axle while a trailing car wheel rolls due to the friction force between the wheel and the rail. For an accelerating train, part of the tractive forces is distributed as the friction forces between the trailing car wheels and the rail. However, as the number of the locomotive wheels much less than that of the trailing railcar wheels, larger longitudinal forces are produced by locomotive wheels. Therefore, an accelerating locomotive wheel is of most importance to be investigated concerning the longitudinal force imparted in the fastening system.

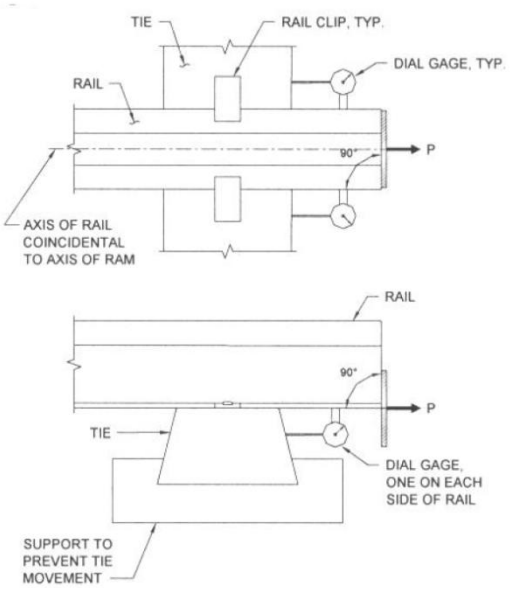

Figure 1. Fastener Longitudinal Restraint Test [4]

In addition to the field experimentation, the mechanical behaviors of a railway track system can also be studied using FE analysis. In a study presented by Nguyen et al. [5], a two-dimensional (2D) and a three-dimensional (3D) FE model were both developed to investigate the response of a railway track under high speed vertical dynamic loading. The 2D FE model utilizes Timoshenko beam elements and spring-dampers and allows for significant savings on the computational cost. However, the 2D model lacks the ability to simulate the behaviors of the fastening components for which the 3D FE model is able to compensate. In another study by Chen et al. [6], a 3D FE model of a track system with detailed fastening components is developed to study the response of the fastening system under combined static vertical and lateral wheel loads. It allows for the investigation of the behaviors of every fastening component. However, the model only considers static loading scenarios which can compromise the accuracy of the results considering the dynamic effects. As few FE models have been developed for investigating the behaviors of longitudinal force in the railway track system, a 3D dynamic FE model is needed in order to gain insights into this subject.

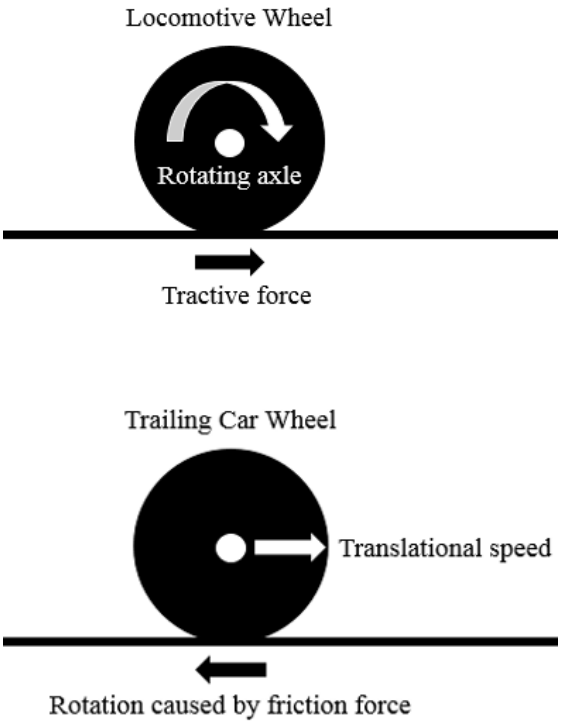

Figure 2. Difference in Driving Mechanisms between a Trailing Car and a Locomotive Wheel

The FE study presented in this research applies an improved 3D FE model of a railcar wheel-track system. It highlights a 26.2-m length of railway track consisting of detailed 3D fastening components. The extensive length of the track system ensures that little longitudinal force is present in the fastening system at the boundary locations. Field experimental data was used to validate the FE model. The FE modeling results are used for the investigation of the behaviors of longitudinal force in the fastening system with different system parameters which include the accelerating rate of the wheel, the elastic modulus of the clips, the COF between the rail and the rail pads, and the spacing of the sleepers.

II. FE Model Development

2.1. FE Model Overview

In order to gain insight into the behavior of the fastening system under dynamic longitudinal wheel load, a FE model was developed using commercial software ABAQUS [7]. The FE model simulated the rolling of a locomotive wheel on a finite length of a railway track. As previously mentioned, the maximum longitudinal wheel load is imparted from an accelerating locomotive wheel, thus the FE model only considered a locomotive

wheel.

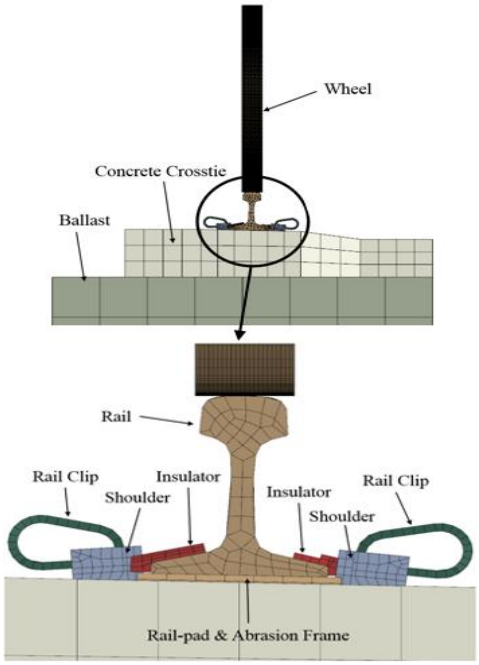

Figure 3 shows the wheel and the cross-section of the track system in the FE model.

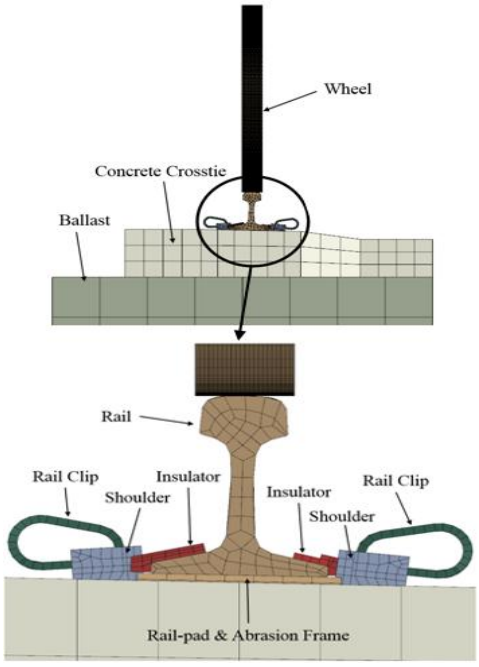

Figure 3. Schematic View of the FE Model

The FE model included a tangent track with a locomotive wheel. As the tangent railway track was symmetric about its center, the FE model only concerned half of the track system, which significantly reduced the computational cost. The wheel-rail contact interaction was simplified so that it only concerned the contact between the wheel tread and rail [8]. The wheel flange and rail contact was deemed to have little effect on track longitudinal response, thus the wheel flange was neglected in the FE model. Therefore, as illustrated in

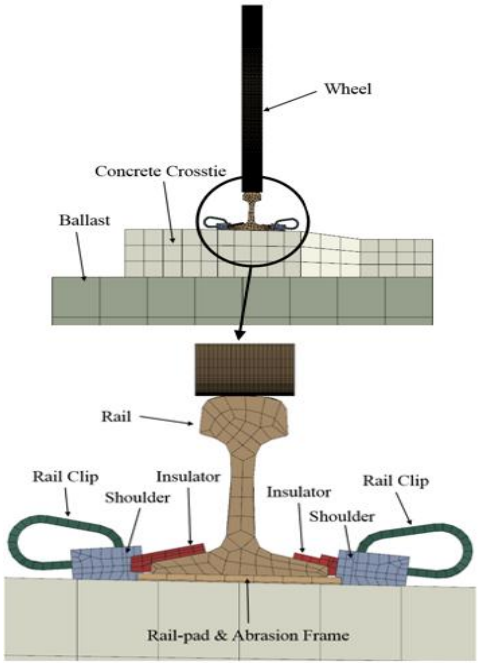

Figure 3, the wheel was modeled as a circular plate which represented the wheel tread and web. In the modeled track system, 136 RE rails, Safelok I fastening systems and concrete sleepers were used. The Safelok I fastening system included a rail clip, shoulder, rail pad assembly (i.e. rail pad and abrasion frame), and insulator (

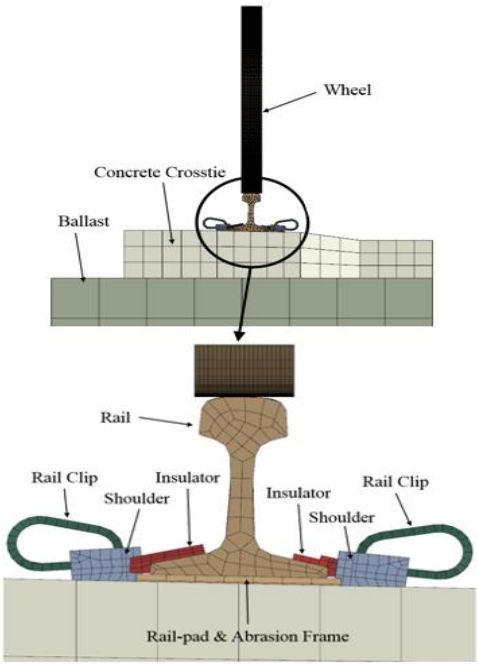

Figure 3). The detailed FE model of each track component is described in greater detail in [6].

The modeled track, as shown in **Error! Reference source not found.**, consisted of 43 sets of sleepers and fastening systems with uniform sleeper spacing of 0.61 m, summing to

26.2 m of track. The track was composed of three parts: an 11.0-m segment at the left end, a 4.2-m segment at the center, and another 11.0 segment the right end. One of the purposes of the end segments was to ensure that, as the wheel rolled over the center segment, the ends of the rails were not affected by the rail flexural bending under vertical wheel load [9]. In addition, as the rail is much stiffer longitudinally than transversely, longitudinal force remains more significant than vertical (transverse) force beyond the region affected by vertical wheel loads [10]. The extended length of the end segments allowed for the fastening system located at the boundaries to experience little longitudinal force. In other words, the two end segments served as boundary conditions to the center segment.

2.2. Element Type Assignments and Mesh Size

All track components were modeled as 3D deformable solids except for the prestressing strands and the wheel. The prestressing strands were modeled using two-node linear beam elements in the sleepers and the wheel was modeled as a rigid body. Because the element size at the contact interface between the wheel and rail is expected to have a significant effect on the accuracy of the output vertical contact force between the two contact bodies during dynamic simulation, refined elements were used on the railhead for the 4.2-m rail segment. Elements were used for mesh transition from the refined contact interface to the rest of the rail (Figure 5). Similarly, refined elements were implemented on the perimeter of the wheel tread with a transition to coarser elements towards the center of the wheel.

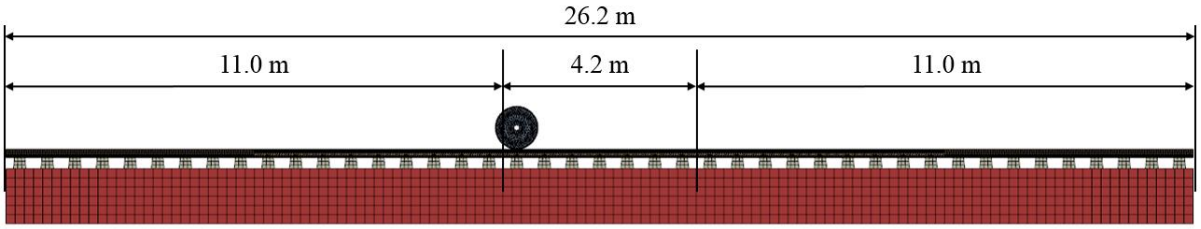

Figure 4. FE Model Track Overview (Profile View)

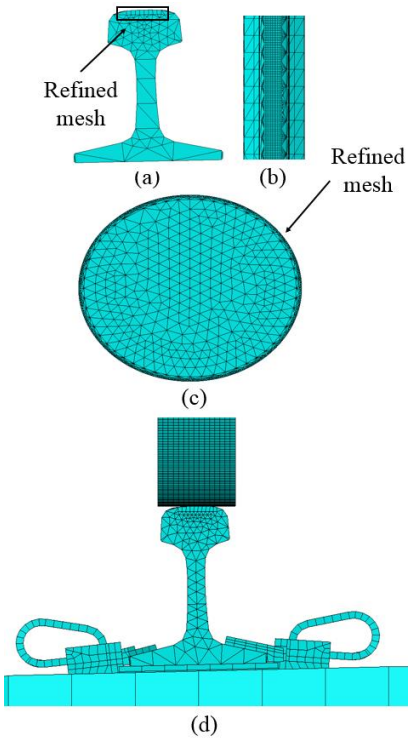

Figure 5. (a) Cross-section View of the Center Rail; (b) Top view of the Center Rail; (c) Wheel; (d) Wheel-rail Contact Interface

In the FE model, the longitudinal force produced by the accelerating wheel is related to the mass of the wheel. However, the wheel, modeled as a rigid body, is massless and therefore a point mass was assigned to the center of the wheel. The value of the mass was calculated based on the total weight of the particular passenger train used in the field experimentation such that the longitudinal wheel load per locomotive wheel in the FE model complied with that in the field experimentation.

2.3. Constitutive Relationships

The material property of concrete was defined using concrete damaged plasticity model that considered two failure mechanisms; tensile cracking and compressive crushing. Under uniaxial tensile loading, concrete exhibited linear-elastic stress-strain relationship until the cracking stress was reached, and, thereafter, strain-softening behavior started to take place. An additional phase, strain-hardening, was present between linear-elastic and strain-softening phases when concrete was under uniaxial compressive loading. The two damage parameters, dt and dc as shown in Figure 6, characterized concrete unloading stiffness and were not defined in the model as cyclic loading was not included in the model [6]. The important variables used to define the constitutive behavior of concrete are summarized in Table *1*.

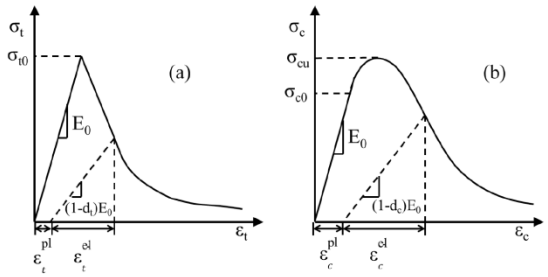

Figure 6. Stress-strain Relation of Concrete in (a) Tension and (b) Compression [7]

In the field, a track substructure is composed of multiple layers that include ballast, subballast, and subgrade. Given that the substructure is largely made up of discrete particles, they can be modelled using discrete element method which is able to capture the realistic response of the track substructure [11]. However, as the computational cost imposed by discrete element method was high and the focus of this study was not on the behavior of the track substructure, it was simplified as a single layer of supporting block. The material property incorporated in the FE model was in accordance with field data obtained from the testing track at the Transportation Technology Center (TTC) in Pueblo, CO funded by the Federal Railroad Administration (FRA) [12]. Based on the measurement results, the hyperelastic material model was defined for the substructure (Figure 7).

Table *1* summarizes major material properties associated with each track component. Under compression, the supporting block exhibited a linear stress-strain relation up to a strain value of -0.083%, preceding a nonlinear stress-strain relation thereafter. In the range of nonlinear stress-strain relation, when the stress was increased, the elastic modulus increased as the supporting block hardened.

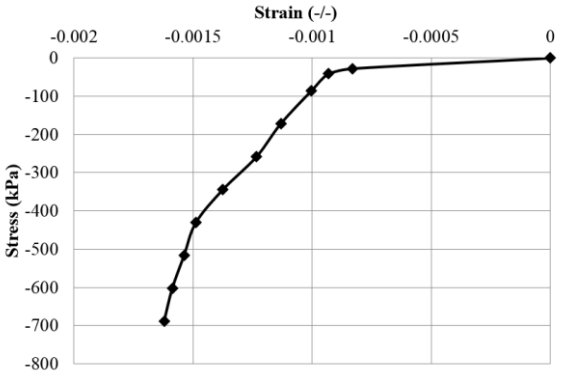

Figure 7. Stress and Strain Relation for Track Substructure under Compression

In the FE model, the plastic behavior of rail steel was neglected as the response of the rail was expected to be linear. Therefore a linear-elastic stress-strain relationship was employed to describe the material behavior of rail.

The field-side insulator is made of two materials; thus it has two material properties listed.

Table 1. Material Properties for Each Track Component

Component	Density (kg/m3)	Young's Modulus (kPa)	Poisson's Ratio	Yield Strength (kPa)	Ultimate Strength (kPa)	Ultimate Strain
Abrasion frame	1137.53	3.03E+06	0.35	8.27E+04	N/A	N/A
Ballast	27609.90	N/A	0.4	N/A	N/A	N/A
Clip	7830.17	1.59E+08	0.29	1.26E+06	1.39E+06	0.05
Sleeper	2300.83	3.00E+07	0.2	2.43E+04	4.83E+04	0.00143
Field-side	1137.53	3.03E+06	0.35	8.27E+04	N/A	N/A
Insulator	7830.17	1.69E+08	0.3	3.10E+05	4.48E+05	0.01
Gauge-side Insulator	1137.53	3.03E+06	0.35	8.27E+04	N/A	N/A
Rail	8006.87	2.07E+08	0.3	N/A	N/A	N/A
Rail pad	1016.04	5.17E+04	0.394	3.59E+04	N/A	N/A
Shoulder	7830.17	1.69E+08	0.3	3.10E+05	4.48E+05	0.01
Strand	8006.87	2.23E+08	0.3	1.76E+06	N/A	N/A
Wheel	8006.87	2.07E+08	0.3	N/A	N/A	N/A

2.4. Contact Interactions

Contact interactions between track components were formulated using surface-to-surface contact discretization, and a master and a slave surface were defined for each contact pair. This contact formulation method prevents large and undetected penetrations of nodes on master surface into slave surface, providing more accurate stress and strain results compared to other methods [7]. The basic Coulomb friction model with the penalty friction formulation was used to simulate the frictional force response at the contact interface.

The maximum allowable frictional stress is related to contact pressure by COF between contacting bodies. COF between wheel and rail is a variable with high degree of nonlinearity and is dependent on a variety of field variables, including temperature, humidity, speed, etc. Based on the findings of an experimental study by Wang et al. [13] on the adhesion behavior between wheel and rail, the COF ranges from 0.4 to 0.5 under dry conditions; and the value decreases with increasing speed. As a simplification, a COF of 0.5 between the wheel and rail was used in the FE model. The COFs of other contact pairs in the model were determined from literature [14], [15], [16] and based on a series of large-scale abrasion tests conducted at the University of Illinois [17].

Table *2* summarizes the values of COFs used in the study.

Table 2. COF Input used in the FE Model

Frictional Interaction	COF
Pad-rail interface	0.3
Frame-concrete interface	0.3
Insulator-rail interface	0.15
Insulator-clip interface	0.15
Insulator-shoulder interface	0.15
Shoulder-clip interface	0.5
Sleeper-ballast interface	0.7
Wheel-rail interface	0.5

Contact interaction between the legs of a shoulder and concrete sleeper involves contacts of relatively more complex geometries and was difficult to simulate using conventional contact formulation methods. As the relative movement between the shoulder-insert and concrete sleeper is expected to be negligible, the constraint feature 'embedded region' in ABAQUS provides a convenient approach in modelling the interaction. The elements of shoulder inserts were defined to be embedded in concrete sleeper, and the translational degrees of freedom of nodes on shoulder inserts were constrained by that on concrete sleeper, accurately representing the bond between the two components prior to the occurrence of cracking in concrete sleeper [7].

In reality, some amount of bond slippage occurs between prestressing strands and concrete as the concrete sleeper undergoes bending. However, slippage of prestressing strands is not likely to have significant effects on the behavior of fastening components, hence it is neglected for this analysis. Therefore, the 'embedded region' constraint that allows no bond-slippage between hosting and embedded regions was used to model the interaction between prestressing strands and concrete sleeper.

A reference node was created at the centroid of the wheel to simulate an axle. The translational and rotational degree of freedoms of all nodes on the wheel was bound to that of the reference node. In other words, any rotation and translation of the reference node were transmitted to the wheel.

2.5. Loading Procedure and Boundary Conditions

The FE analysis consisted of two phases. The first phase was the static loading phase that served to stabilize the track system in a static sense before a dynamic simulation. The static analysis phase included prestressing concrete sleepers with strands, clamping clips onto the rail, applying gravity loads to the system, and applying the wheel load. Following the manufacturer's specification, the tensile capacity of all the prestressing strands was 38.9 kN/strand. A prestressing force of 31.1 kN was applied to each of the 20 strands embedded in each concrete sleeper, which was 80% of the tensile strength of a strand. When the prestressing force was released, the deformation of strands would engage concrete with compressive force. In the FE model, the assembly of clips was initiated in the same step. Pressures were first applied to lift up the toes of clips over the insulators. With the pressures applied, clips were then displaced towards the rail and the clip inserts were socketed into the grooves on the shoulders. As the tips of clips were directly placed over insulators, lifting pressure was decreased and the clips clamped onto the insulators. The following step was used to apply gravity loads to the superstructure components of the track system to simulate the resistance to upward deflection resulted from the vertical wheel load. In addition, the wheel load was applied to the reference point of the wheel. Figure 8 illustrates the loading and boundary conditions in each step.

The next phase was the dynamic simulation as shown in Figure 8, Step 7. As the total dynamic step running time was expected to be relatively long, an implicit time integration scheme was selected for the dynamic simulation. To conform to the acceleration of the passenger train in the field experimentation, a rotational acceleration of 0.65 radians/sec2, equivalent to a translational acceleration of 0.12 m/sec2, was applied to the reference node at the center of the wheel in the dynamic simulation step in the FE model. The total step time was deemed sufficiently long for the wheel to pass the center segment of the rail such that enough data points could be collected.

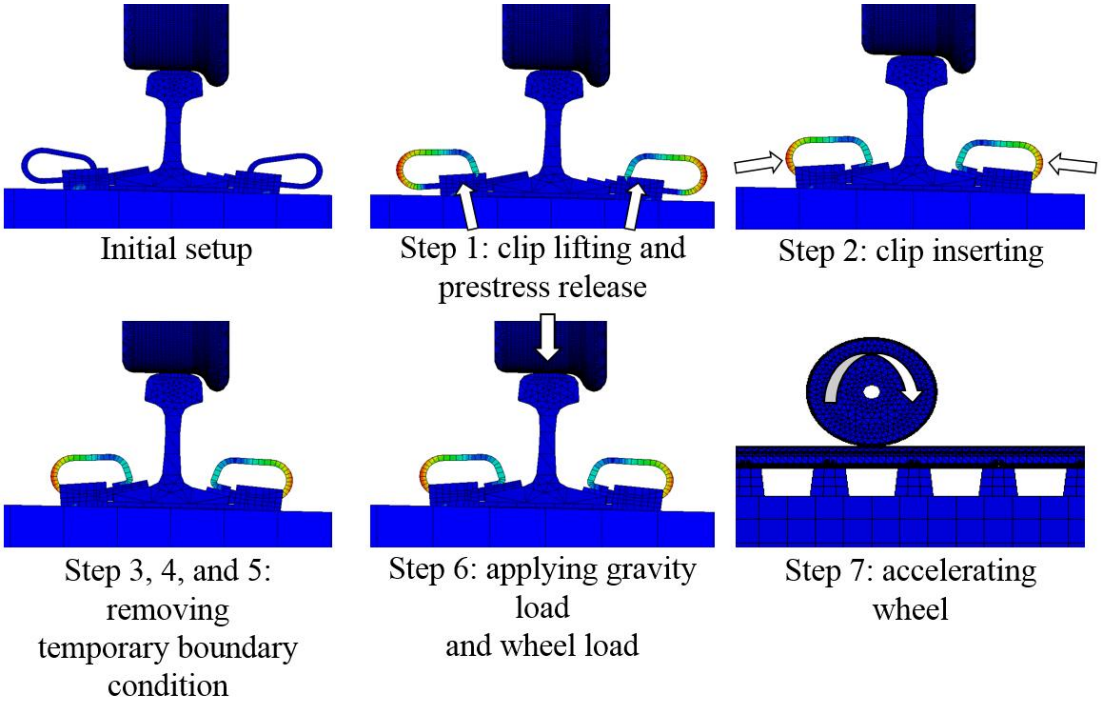

Figure 8. Sequence of Application of Loadings and Boundary Conditions in the FE Model

III. FE MODEL VALIDATION

3.1. Field Test Setup

Field experiments were conducted at TTC in Pueblo, CO, USA. The results from the testing on a tangent track section were used for model validation. For this segment, 15 new concrete sleepers were installed and tamped prior to experimentation, and strain gauges were installed on the rail to record the dynamic wheel loads and rail behavior (Figure 9).

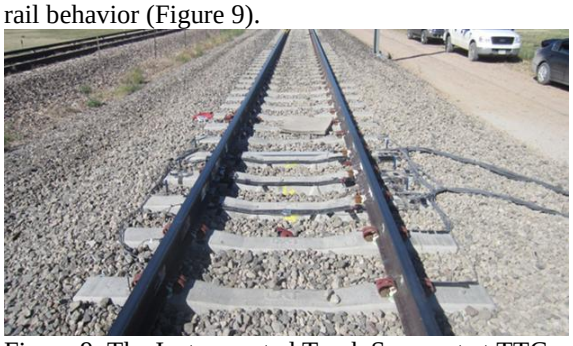

Figure 9. The Instrumented Track Segment at TTC

To examine the rail behavior under the vertical wheel loads, strain gauges were installed in the vertical direction above the rail seats (Figure 10). For the instrumented locations, three gauges were placed in a line on both sides of the rail. To eliminate the effect of lateral wheel loads, the average value measured from the front and back sides of rail was used to compare with the modelling results.

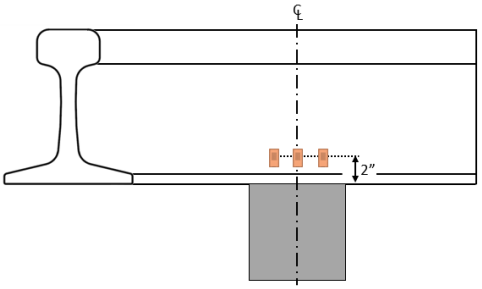

Figure 10. Locations of Vertical Strain Gauges Placed Above Rail Seat

Strain gauges were also installed on the rail web to measure the longitudinal strain in the rail under the passage of the testing train. Chevron patterns, which consisted of two strain gauges placed perpendicular to each other, were installed on the neutral axis of the rail and at the center of the crib (the portion between two sleepers). In addition, linear potentiometers were installed to measure the longitudinal displacement of the rail pad under the influence of longitudinal wheel loads. Figure 11 shows the location of the linear potentiometer; it was placed at the edge of the sleeper such that the tip of it was in contact with the rail pad. Readings recorded from the linear potentiometer that had positive values indicated that the rail pad displaced along the same direction the train was traveling and vice versa.

Figure 11. Linear Potentiometer Placement in the Field Experimentation at TTC

3.2. Field Validation of FE Model

Component–level models and single-sleeper FE models were previously calibrated with field and laboratory experimental results [6]. Therefore, only system level validation was performed for this FE model. The FE model was validated by comparing recorded time histories of three properties: vertical and longitudinal strains in the rail and longitudinal displacement of the rail pad. The validation based on the vertical and longitudinal strains of the rail web ensured that the vertical and longitudinal forces transmitted from the wheel to the rail were physically making sense. And validating the longitudinal displacement of the rail pad in the FE model assured the longitudinal force transferred from the rail to the rail pad was a close approximation of the field condition.

In the FE model, the wheel accelerated from stationary; while, in the field experimentation, the train accelerated past the instrumented section with some initial speed. In other words, the testing data and the modeling data had different time scales. Therefore, side-by-side comparisons were made and the emphasis was on the peak values observed and the shapes of the curves.

3.2.1. Rail Pad Longitudinal Displacement

Based on field and numerical results (Figure 12), the rail pad underwent a positive displacement followed by a negative displacement. As the rail and rail pad were in contact, the moving direction of rail pad always conformed to that of the rail. Therefore, the positive displacement was attributed to the positive longitudinal elongation of rail as a result of Poisson's effect under the influence of vertical wheel load as the wheel approaches (Figure 13). Similarly, the negative displacement was a result of both the negative longitudinal elongation of rail, as illustrated in Figure 13, and movement of rail along the negative direction due to wheel-induced friction force. As shown in Figure 12, the shape of the modeling data well resembled the field data. Field data showed a maximum positive displacement of 0.0234 mm compared to 0.0208 mm from the numerical result, resulting in a reasonable 12.5% difference. The maximum negative displacement in the FE model was -0.0104 mm and was 11.1% less than the field data of -0.0117 mm. The percentage differences were small; therefore, a good agreement between the field and modeling data was realized for the longitudinal displacement of the rail pad.

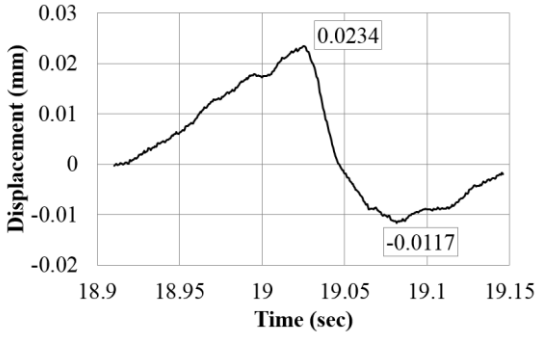

(a)

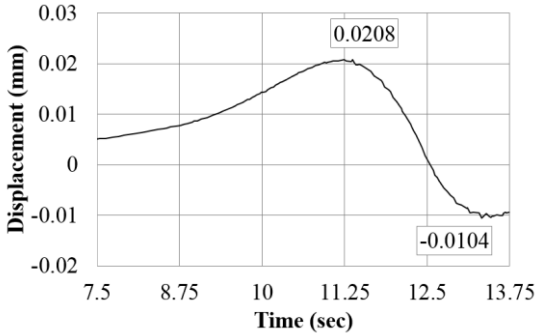

(b)

Figure 12. Comparison between (a) Field Result and (b) Modeling Result for Rail Pad Longitudinal Displacement

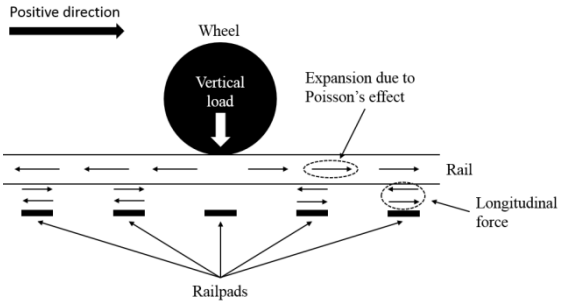

Figure 13. Longitudinal Force at the Rail to Rail Pad Interface due to Vertical Wheel Load

3.2.2. Longitudinal Strain in the Rail

Figure 14 shows the comparison between the field data and FE model data for the longitudinal strain in the rail. In both curves, a minimum value (maximum compression) was proceeded and followed by two positive peak values (maximum tension). The field data gave a maximum compressive strain value that was 6.23% greater than the numerical result. In addition, the FE model gave two maximum tensile strain values that were 20.5% and 13.5% less than the field data,

respectively. Therefore, a considerably good comparison was observed between the field data and the numerical result for the longitudinal strain in the rail.

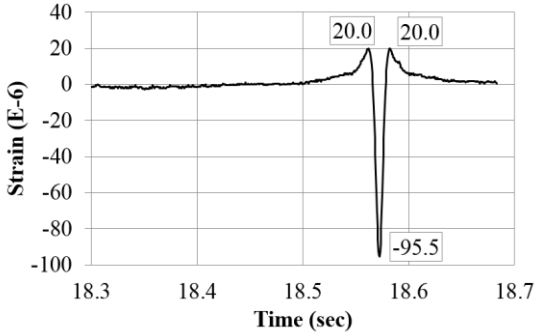

(a)

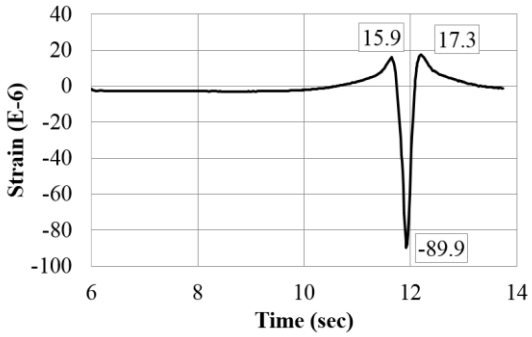

(b)

Figure 14. Comparison between (a) Field Result and (b) Modeling Result for Longitudinal Strain in Rail Web

3.2.3. Vertical Strain in the Rail

The comparison for the vertical strain in the rail is shown in Figure 15. The shapes of the two curves exhibited similarities to a high extent. Both the field and the modeling data decreased and reached a maximum compressive strain as the wheel approached, indicating a compressive load in the rail, and started to increase after the passage of the wheel. The FE model gave a maximum compressive strain value of -0.142 millistrain which was 2.16% different from -0.139 millistrain recorded from the field. Therefore, the comparisons between the numerical solutions and the field data demonstrated that the FE model was capable of representing longitudinal behaviors of the railway track structure under a dynamic wheel loading; thus, the validated FE model could be used for further analysis.

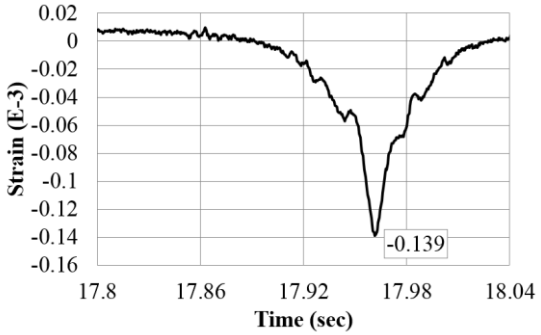

(a)

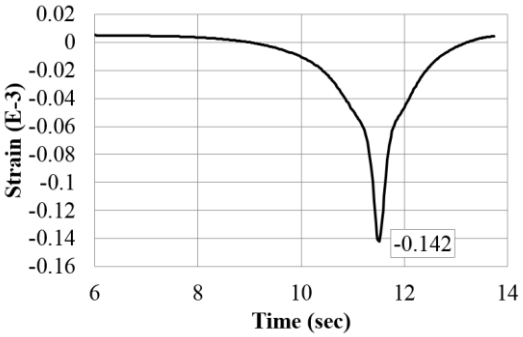

(b)

Figure 15. Comparison between (a) Field Result and (b) Modeling Result for Vertical Strain in Rail

IV. PARAMETRIC STUDY

A parametric study was conducted using the validated FE model. The parameters include the acceleration of wheel, elastic modulus of the clips, COF between the rail and rail pads, and spacing between sleepers.

4.1. Acceleration

The acceleration of a train is highly dependent on the power of its locomotives, the total weight of the train, and the maximum adhesion between the locomotive wheels and rail. In order to investigate cases with varying longitudinal force between the wheel and rail, accelerations of 0.12 (field acceleration), 0.32, 0.51, and 0.76 m/sec2 were considered in the study.

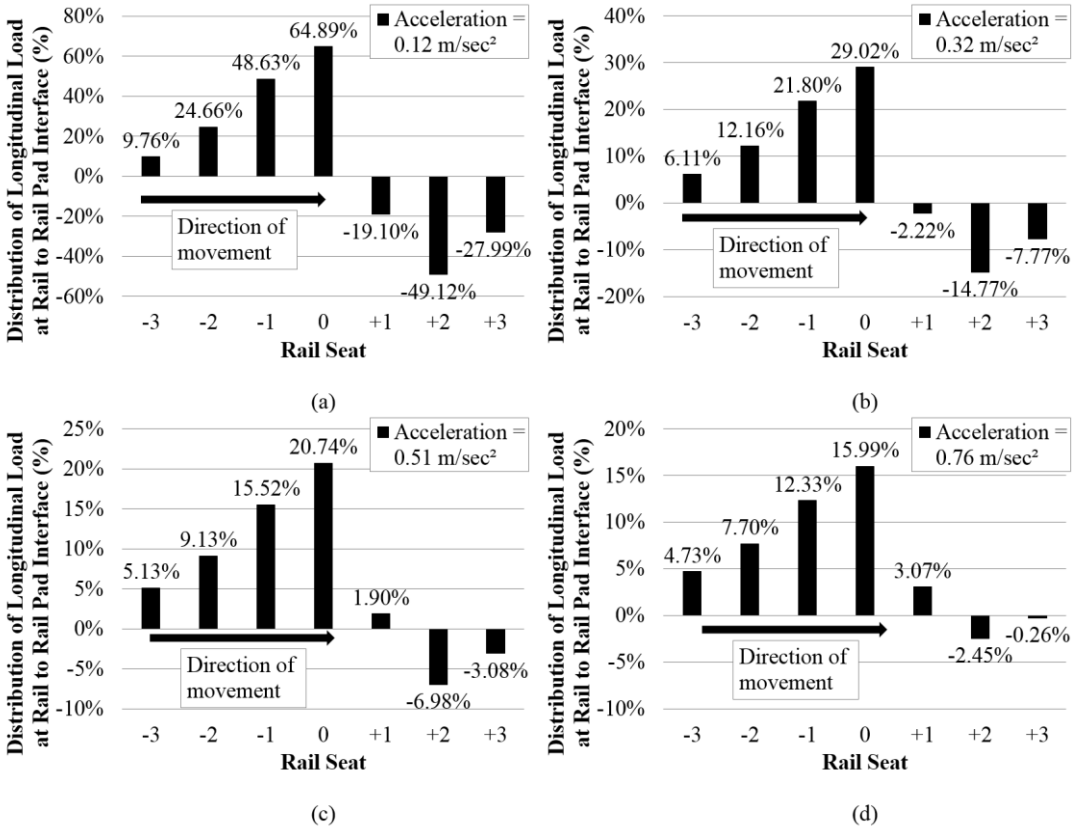

Figure 16. Distribution of Longitudinal Load for Rail to Rail Pad Interfaces at the Center Seven Sleepers at Wheel Accelerations of (a) 0.12 m/sec2, (b) 0.32 m/sec2, (c) 0.51 m/sec2, and (d) 0.76 m/sec2

Figure 16 compares the percent distributions of longitudinal load between the rail and rail pads (on the bottom of the rail) for the center seven rail seats for the four different cases of wheel accelerations. Positive values indicated that the force was in the same direction as the movement of wheel. The rails seat numbered zero is the 22nd rail seat located at the center of the modeled track (**Error! Reference source not found.**). It could be observed that the longitudinal force was more concentrated at the rail seats in the vicinity of the wheel at low acceleration. As wheel acceleration increased, the distribution became less skewed towards the center rail seat. Higher accelerations caused the rail to displace more in its longitudinal direction, imparting more longitudinal force to the far rail seats.

The values of percent distribution were negative at the rail seats where the rail pad exerted longitudinal force opposite to the direction the wheel traveled on the rail. This observation can be explained by Figure 12. Before the wheel reached a rail seat, the longitudinal displacement of the rail pad was positive (same direction as the movement of wheel), hence a positive longitudinal force on the rail pad from the rail. Therefore, the longitudinal force exerted on the bottom of the rail by the rail pad was negative. As shown in Figure 16, the percent distribution of the negative forces decreases with increasing wheel accelerations. The reason was that higher wheel accelerations caused the rail to displace more towards the negative direction, therewith reduced the positive displacement resulted from the effect of vertical bending.

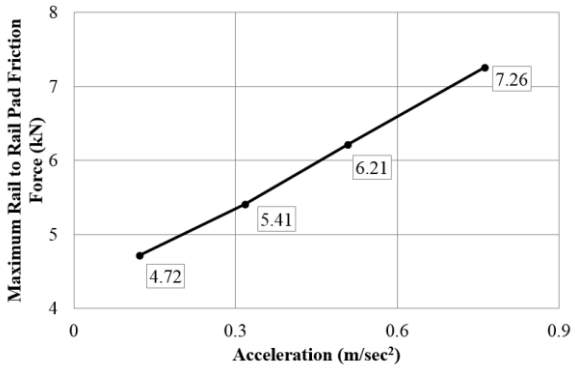

Figure 17. Relationship between Acceleration and Maximum Friction Force at Rail to Rail Pad Interface

In addition to the percent distribution of the longitudinal force between the rail and rail pad, the relationship between its maximum value and the wheel acceleration was also investigated. As shown in Figure 17, the maximum longitudinal force at the rail to rail pad interface increases

linearly with wheel acceleration. However, the percent increase in the maximum longitudinal force was only 54% while the acceleration increased by more than five times. It agreed with Figure 16 that the percent distribution decreased at the center rail seat even though the force transmitted to it increased; and this behavior could be attributed to the high rigidity of the rail in the longitudinal direction. In other words, the majority of the longitudinal force produced by the wheel at high accelerations was distributed to the far rail seats.

4.2. Elastic Modulus of Rail Pad

The modulus of elasticity of the clips has a direct effect on the clamping force applied on the rail which is related to the capacity of longitudinal restraint a rail seat has. Four elastic moduli; 138, 159, 179, and 200 GPa; were simulated in the FE model. Figure 18 compares the percent distributions of longitudinal load between the rail and rail pads for the center seven rail seats for the four different cases of the elastic moduli of clips. The difference in the distribution of longitudinal forces was not inconspicuous among the four cases. A modulus of elasticity of 179 GPa lead to the highest percent distribution of longitudinal force at the center rail seat, but only surpassed the lowest value by a negligible difference. Therefore, the elastic modulus of clips had almost no effect on the distribution of longitudinal forces among rail seats.

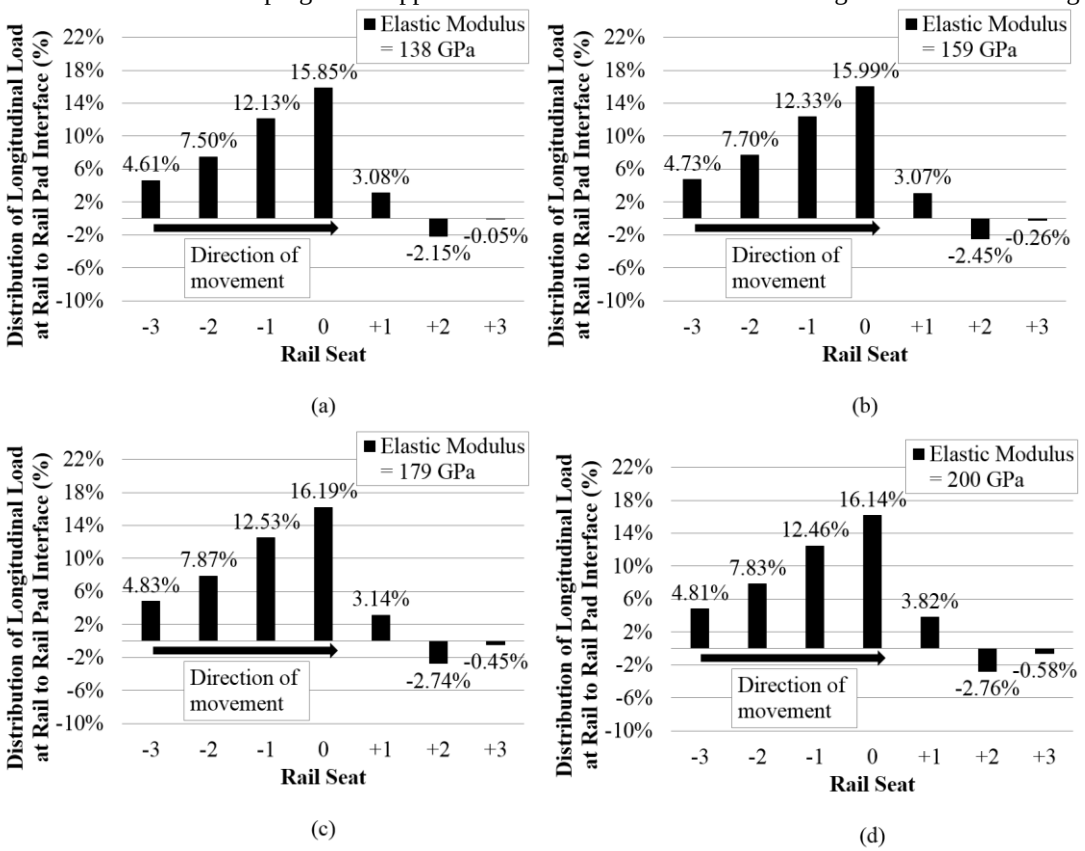

Figure 18. Distribution of Longitudinal Load for Rail to Rail Pad Interfaces at the Center Seven Sleepers with Clip Elastic Modulus of (a) 138 GPa, (b) 159 GPa, (c) 179 GPa, and (d) 200 GPa

The relationship between the maximum longitudinal force at the rail to rail pad interface and modulus of elasticity of clips is illustrated in Figure 19. Similar to the observations for the distribution of longitudinal forces, there was almost no changes in the maximum force as the elastic modulus of clips was varied. Additionally, Figure 19 suggested that the design of clips could be too conservative as, for this particular train, reducing the elastic modulus from the design value of 159 GPa to 138 GPa would barely deprive the capacity of longitudinal restraint of fastening system.

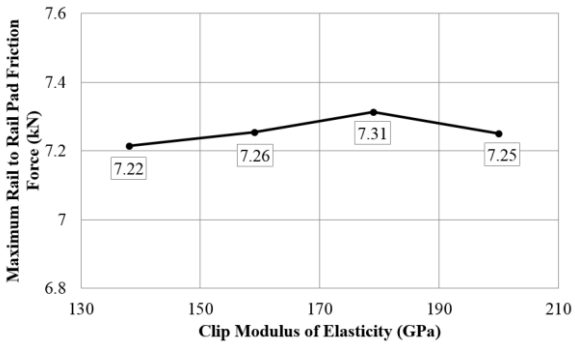

Figure 19. Relationship between Clip Elastic Modulus and Maximum Friction Force at Rail-rail pad Interface

4.3. Rail to Rail Pad Coefficient of Friction

The COF for the contact pair of rail and rail pad has a direct effect on the longitudinal restraint a rail seat can provide. The COF for the contact between the rail and rail pad has a range between 0.12 and 1.5 [14], [16], [18]. A total of four COFs; 0.15, 0.30, 0.65, and 1.0 were simulated in the FE model. A COF of 0.15 considered a wet surface condition whereas a COF of 0.30 considered a dry surface condition [16]. The values of 0.65 and 1.0 were included to account for the introduction of various degrees of roughness on the surface of rail pads [18]. As shown in

Figure *20*, the percent distribution of longitudinal force at the center rail seat exhibited a considerable increase with COF up to 0.65. No significant change was observed as the COF was raised from 0.65 to 1.0. Therefore, considering the additional efforts required to produce a rougher surface, a COF of 0.65 was deemed most efficient for providing longitudinal restraint for a rail seat.

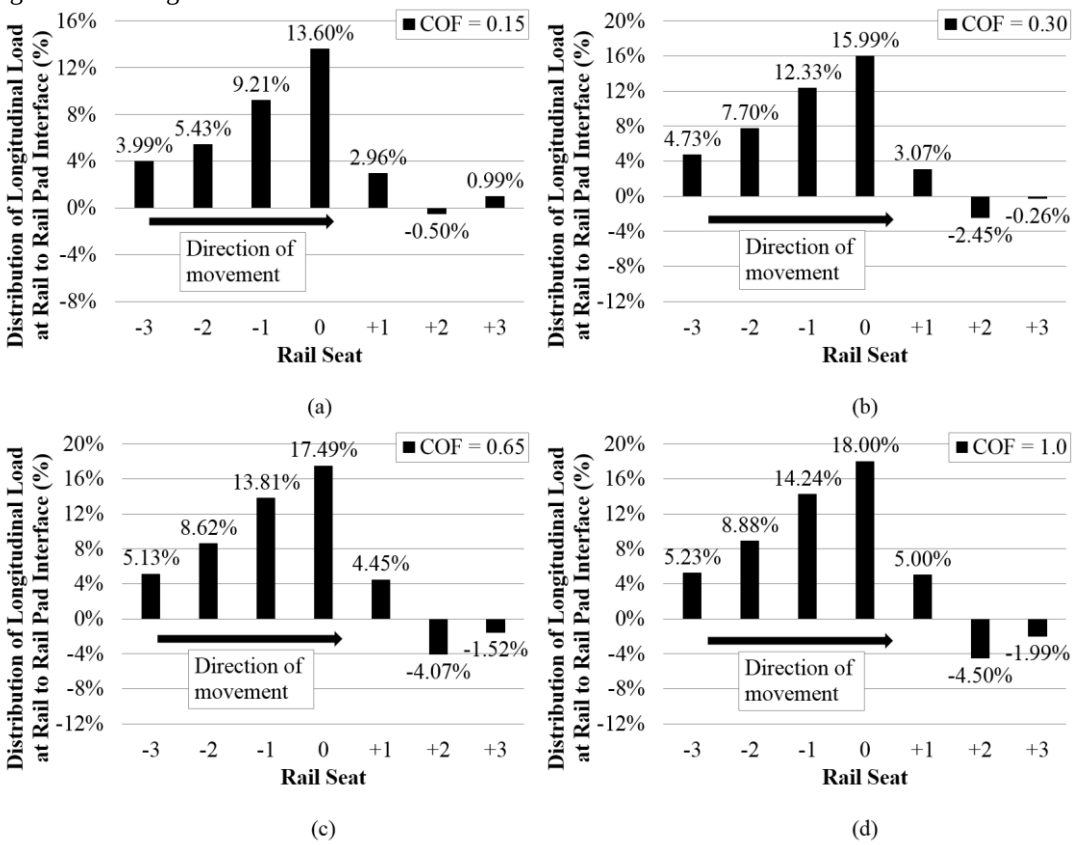

Figure 20. Distribution of Longitudinal Load for Rail to Rail Pad Interfaces at the Center Seven Sleepers with Rail to Rail Pad COF of (a) 0.15, (b) 0.30, (c) 0.65, and (d) 1.0

The relationship between the maximum longitudinal force at the rail to rail pad interface and COF between the rail and rail pads is presented in Figure 21. The maximum force increased with COF; nonetheless, the rate of increase decreased at high COFs. From a COF of 0.15 to 0.30, the maximum force increased by 20% whereas a mere 3.7% increase in the maximum force was obtained as the COF increased from 0.65 to 1.0. The observations in Figure 21 agreed with those in

Figure *20* as the gains in the capacity of longitudinal restraint at a rail seat was not cost-effective beyond the COF of 0.65.

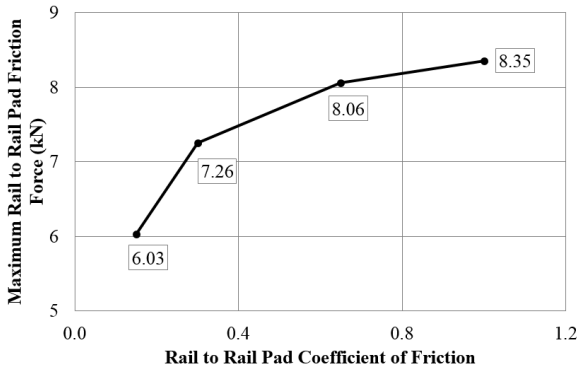

Figure 21. Relationship between Rail to Rail Pad COF and Maximum Friction Force at Rail-rail pad Interface

4.4. Sleeper Spacing

For concrete sleepers, the center-to-center spacing of sleepers in typical practice ranges between 0.51 m and 0.76 m [4]. The sleeper spacing of the test track in the field experimentation was 24 inches which fell in the middle of the code-specified range. Two additional cases, 0.51- and 0.76-m spacing, were investigated in the FE model to reveal the effects of sleeper spacing on the distribution of longitudinal force.

For sleeper spacing of 0.51 and 0.61 m, the distributions of longitudinal force were similar (Figure 22). Small increase was observed at the center rail seat while the adjacent rail seats underwent small decrease in percent distribution. Nevertheless, a more considerable increase, 24%, only took place at the center rail seat as the spacing increased from 0.61 to 0.76 m whereas the distributions at other rail seats remained almost the same. The sole increase at the center rail seat is deemed related to the increase in vertical loads experienced by the rail seats in the vicinity of the wheel due to larger sleeper spacing. Therefore, considering the three sleeper spacing simulated in the FE model, the 0.61-m spacing ensured the most uniform distribution of longitudinal force without requiring too small of a spacing.

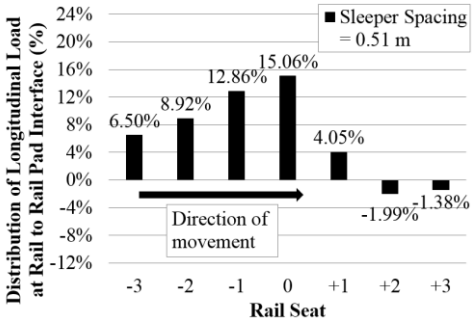

(a)

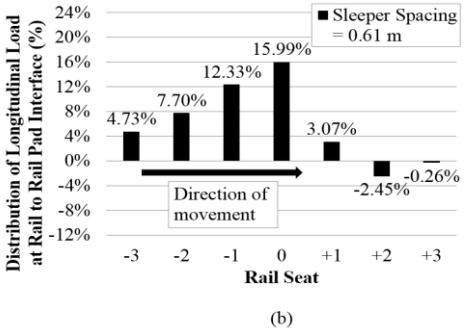

(b)

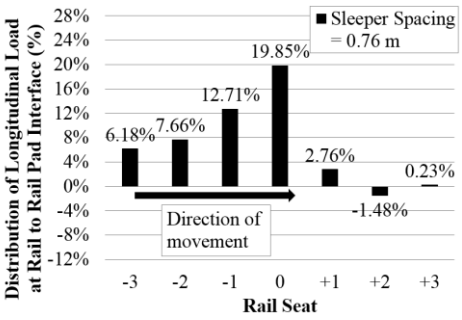

(c)

Figure 22. Distribution of Longitudinal Load for Rail to Rail Pad Interfaces at the Center Seven Sleepers with Sleeper Spacing of (a) 0.51 m, (b) 0.61 m, and (c) 0.76 m

Based on Figure 23, the maximum longitudinal force resembled an exponential growth as the sleepers were spaced further apart. In other words, increasing the spacing of sleepers could potentially impose a severe increase in the demand for longitudinal restraint of fastening system. Therefore, the relationship between the maximum rail to railpad longitudinal force and sleeper spacing suggested the significance of imposing an upper limit on the spacing of sleepers.

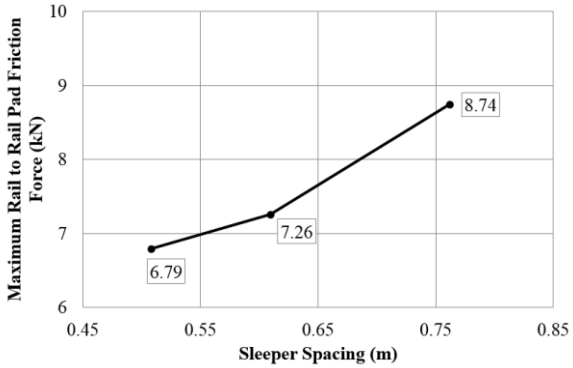

Figure 23. Relationship between the Spacing of Sleepers and Maximum Friction Force at Rail-rail pad Interface

V. CONCLUSIONS

A field validated 3D FE model was developed to study the distribution of longitudinal force in the fastening system of railway track, particularly at the interface between the rail and rail pad. The effects of four groups of parameters; including the acceleration of wheel, modulus of elasticity of clips, COF between the rail and rail pad, and spacing of sleepers; on the longitudinal force distribution as well as on the maximum value of longitudinal force were investigated. Based on the results of parametric study, it can be realized that:

- As the acceleration of wheel increases, the distribution of longitudinal force becomes less skewed as the maximum percent distribution decreases and a larger portion of the longitudinal force is distributed to the far rail seats beyond the center seven.
- The maximum longitudinal force between the rail and rail pad increases linearly with wheel acceleration.
- The modulus of elasticity of clips has little effect on the distribution of longitudinal force, suggesting the potential surplus in the elastic modulus of clips regarding the demand for longitudinal restraint.
- The increase in COF between the rail and rail pad causes a larger portion of the longitudinal force to converge to the center rail seat, essentially increasing the capacity of longitudinal restraint of fastening system. Additionally, a COF of 0.65 is deemed most efficient in maximizing the longitudinal restraint provided at a rail seat.
- Significant increase in the distribution of longitudinal force at the center rail seat takes place as the sleeper spacing increases beyond 0.61 m, suggesting that 0.61-m spacing for sleepers facilitates the most uniform distribution of longitudinal force without requiring unreasonably small sleeper spacing.
- The maximum longitudinal force between the rail and rail pad increases exponentially with the spacing of sleepers.

VI. ACKNOWLEDGEMENTS

The United States Department of Transportation (US DOT) Federal Railroad Administration (FRA) and the National University Rail (NURail) Center funded this research project. The published materials in this paper represents the position of the authors and not necessarily that of DOT. Senior Research Engineer Marcus S. Dersch from the UIUC Rail Transportation and Engineering Center (RailTEC) has provided important guidance and support for this project.

REFERENCES

[1] Srinivas, V., Ramanjaneyulu, K., Kumar, K. S., Parivallal, S., Kesavan, K., Ravisankar, K., Lakshmanan, N., & Iyer, N. R. (2013). *Evaluation of Longitudinal Force on a Railway Bridge Based on Strain Measurements.* Experimental Techniques, 55-67.

[2] Foutch, D. A., Kim, T., Otter, D. E., & Doe, B. E. (2006). *Investigation of Longitudinal Forces in a Concrete Railroad Trestle.* Journal of Bridge Engineering, 11(5), 618-625.

[3] *Railway Applications - Track - Test Methods for Fastening System Part 1: Determination of longitudinal rail restraint. (2002).* In Standard EN1314601:2002. Brussels: Comitée Européen de Normalistion (CEN).

[4] AREMA. (2014). *Manual for Railway Engineering.* Lanham, MD 29706: AREMA.

[5] Nguyen, K., Goicolea, J. M., & Galbadon, F. (2011). *Dynamic Analysis of High Speed Railway Track Loads on Ballasted Track.* Proceedings of the Fifth International Symposium on Environmental Vibration. Chengdu, China.

[6] Chen, Z., Shin, M., Andrawes, B., & Edwards, J. (2014). *Parametric study on damage and load demand of prestressed concrete crosstie and fastening systems.* Engineering Failure Analysis, 49-61.

[7] Dassault Systemes Simulia Corp. (2013). *ABAQUS Analysis User's Manual, Version 6.13.*

[8] Anderson, E., Berg, M., & Stichel, S. (2004). *Rail Vehicle Dynamics.* KTH Railway Technology.

[9] Selig, E., & Waters, J. (1994). *Track geotechnology and substructure management.* London: T. Telford.

[10] Rhodes, D., & Coats, B. (2008). *Resistance to rail creep – what do rail fastenings really have to do?* Proceedings of the AREMA 2008 Annual Conference. Salt Lake City, UT.

[11] Huang, H., & Tutumluer, E. (2011). *Discrete Element Modeling for Fouled Railroad Ballast.* Construction and Building Materials, 3306-3312.

[12] Grasse, J. S. (2013). *Field Test Program of the Concrete Crosstie and Fastening System (M.S. Thesis).* Urbana, IL 61801: University of Illinois at Urbana-Champaign.

[13] Wang, W. J., Shen, P., Song, J. H., Liu, Q. Y., & Jin, X. S. (2011). *Experimental Study on Adhesion Behavior of Wheel/Rail under Dry and Water Conditions.* Wear, 2699-2705.

[14] Friedrich, K. (1986). *Friction and wear of polymer composites.* Amsterdam: Elsevier.

[15] Stachowiak, G., & Batchelor, A. (2005). *Engineering tribology (3rd ed.).* Amsterdam: Elsevier Butterworth-Heinemann.

[16] Yamaguchi, Y. (1990). *Tribology of plastic materials: Their characteristics and applications to sliding components.* Amsterdam: Elsevier.

[17] Kernes, R. G., Edwards, J. R., Dersch, M. S., Lange, D. A., & Barkan, C. P. (2012). *Investigation of the Dynamic Frictional Properties of a Concrete Crosstie Rail Seat and Pad and Its Effect on Rail Seat Deterioration (RSD).* Proceedings of the Transportation Research Board 91st Annual Meeting. Washington, D.C.

[18] Bely, V. A., Sviridenok, A. I., & Petrokovets, M. I. (1982). *Friction and Wear in Polymer-Based Materials.* Elsevier.